Available online at www.sciencedirect.com
ScienceDirect
Catalysis Today 118 (2006) 104–112
CATALYSIS TODAY
www.elsevier.com/locate/cattod

Can a fuel-cell stack and an enzyme electro-membrane reactor be combined into a multi-functional unit?

R. Kukul'a [a], P. Hasal [a,*], T. Schultz [b], T. Schröder [b], K. Sundmacher [b]

[a] *Department of Chemical Engineering, Institute of Chemical Technology, Prague, 166 28 Praha 6, Czech Republic*
[b] *Max-Planck-Institute for Dynamics of Complex Technical Systems, 391 06 Magdeburg, Germany*

Available online 5 July 2006

Abstract

First results of an attempt to integrate an electro-membrane enzyme reactor with a fuel-cell stack in order to construct a multi-functional unit are presented. The experimental fuel-cell stack consists of nine single polymer electrolyte membrane fuel cells (with active cross-sectional area of 26 cm^2) consuming pure humidified hydrogen as the fuel. The stack is designed to deliver steady electric power of 30 W (stack voltage of about 6 V at current of about 5 A). The electro-membrane enzyme reactor is composed of five flat-shaped compartments: the cathode and the anode compartments, two reactant stream compartments and the gel slab compartment. The active area of all the compartments is 9 cm^2. The operating curves (current–voltage and power–current curves) of both sub-units and their dynamical behaviours have been measured over a wide range of operating conditions. A comparison of the operating curves of the fuel-cell stack and of the electro-membrane reactor confirmed that these sub-units are electrically compatible and can be mutually integrated within a multi-functional unit, whilst the fuel-cell stack provides enough electrical energy to power also the necessary auxiliary equipment (pumps, blowers, etc.).

Keywords: Multi-functional unit; Electro-membrane reactor; Biotransformation; Fuel cell stack

1. Introduction

The usage of the term *multi-functional reactor* as a synonym for a reactor system that integrates two or more unit operations and necessary equipment into a single unit was proposed in their seminal paper by Agar and Ruppel [1] and later on re-introduced by Westerterp [2]. The concept of multi-functionality can be, however, traced back to the 1940s, when a reactor incorporating catalyst regeneration by coke combustion and heat transfer for an endothermic reaction leading to an autothermal operation was described [3,4]. For a long time autothermal reactors have represented the only group of multi-functional reactors that have found applications on a production scale. Later, reactive distillation became a representative for multi-functional reactors [5]. The term multi-functionality has gradually come to maturity and is nowadays supposed to include the integration of a reaction (biotransformation) with other process operations (unit operations) to manipulate the concentration and/or temperature fields in multi-functional equipment.

Various aspects of multi-functionality were reviewed by a number of authors, e.g., by Hoffman and Sundmacher [6], Agar [7], Dautzenberg and Mukherjee [8] and Stitt [5]. Despite the long history and considerable academic and industrial effort, multi-functional reactors have been applied to relatively few manufacturing applications: reactors for syngas and hydrogen generation, toluene disproportionation by reactive distillation and unsteady state regenerative heat exchange reactors [5]. Catalytic membrane reactors and bioreactors form a group of reactors particularly suitable for an integration to multi-functional systems as they on their own meet a number of

Abbreviations: e1, e2, electrodes; ec1, ec2, electrode compartments; EMER, electro-membrane enzyme reactor; FCS, fuel-cell stack; gsk, gaskets; iem, ion-exchange membrane; MEA, membrane-electrode assembly; MFU, multi-functional unit; PAA, polyacrylamide; PEM, proton exchange membrane; PEMFC, proton exchange membrane fuel cell; rc1, rc2, reactant stream compartments

* Corresponding author. Tel.: +420 220 443 167; fax: +420 220 444 320.
E-mail address: Pavel.Hasal@vscht.cz (P. Hasal).

0920-5861/$ – see front matter © 2006 Elsevier B.V. All rights reserved.
doi:10.1016/j.cattod.2005.11.092

Nomenclature

c_b	buffer concentration (mol dm^{-3})
d_h	hydraulic diameter (m)
i	electric current density (A m^{-2})
I	electric current (A)
P	electric power (W)
Q	volumetric flow rate (m^3 s^{-1})
Re	Reynolds number
U	voltage (V)
U_f	voltage applied to the fan (V)

Greek letters

κ_b	electrolytic conductivity of buffer (mS cm^{-1})
η	dynamical viscosity (Pa s)
ρ	density (kg m^{-3})

Subscripts

b	buffer
f	fan
H_2	hydrogen stream

features demanded from the multi-functional systems [9]. Typically, a reaction or a biotransformation is carried out in a specialized reaction compartment of the membrane reactor and the other compartments fulfill other specific tasks, for example the separation and purification of reaction products, the controlled dosage of reaction components, etc.

Transport processes in the membranes (mostly governed by molecular mechanisms) are characteristically slow and they often lower the overall rate of the production processes taking place in the membrane reactor. Recently we have applied [10–14] a new concept of controlling transport rates in the membrane reactors—an application of electric fields. The electric fields applied to membranes (gel slabs) with the immobilized enzymes result in electrophoretic migration and/or the electro-osmotic flux of reaction components and intra-membrane concentration fields are altered in a way that may lead to the reaction rate enhancement [10,11]. The rate and direction of these two transport mechanisms are controlled by the intensity and orientation of the applied electric field. Mutual interactions of all kinds of mass transport with nonlinear kinetics of enzyme reactions may result in a variety of reaction regimes within the membrane bearing the immobilized enzyme.

The existence of a multiplicity of steady states, hysteresis and sustained oscillations was predicted by mathematical modeling of the electro-membrane reactors where penicillin G hydrolysis by means of the immobilized penicillin G acylase takes place [10–12]. An easy control of the reactor performance by proper time variations of the intensity of the electric field, e.g., by periodic pulses or by ramped voltage applied to the enzyme slab, was demonstrated together with the possibility of compensating for the decaying enzyme activity by proper adjustments of the dc voltage applied to the reactor.

The experiments with two laboratory-scale electro-membrane enzyme reactors (EMERs) operated either in the circulation (batch) mode [13] or in the continuous flow-through mode [14] confirmed the predictions provided by mathematical modeling. Strong dependence of the substrate conversion and a degree of separation of reaction components on the intensity of the electric current was observed in both reactors. The transports of hydrogen and hydroxyl ions within the gel slab, controlled by the applied electric current, were identified as the principal factors controlling the biotransformation rate as these ions control the pH-value field in the slab. The electric current density applied to the reaction compartment in both experimental EMERs was varied from +125 to −62.5 mA cm^{-2}.

There has been sustainable effort during last few decades devoted to miscellaneous aspects of the fuel cells and the fuel-cell stacks (FCS), see, e.g., Kordesh and Simander [15] or Larminie and Dicks [16]. Proton exchange membrane fuel cells (PEMFCs) consuming gaseous hydrogen or methane or liquid fuels, as an aqueous methanol solution, are most frequently used in portable devices owing to their simple and versatile constructional arrangements and low (or moderate) operating temperature. The typical operational features of the PEM fuel cells predetermine them as the most appropriate candidates for an integration with electro-membrane enzyme reactors to novel multi-functional units where the fuel cell generates the electric current controlling the biotransformation rate in the coupled enzyme membrane reactor.

The integration of the fuel cell and the electro-membrane enzyme reactor to a single compact unit brings about advantages that are common for all multi-functional reactors, however, it brings additional advantages resulting from the application of the electric field to the enzyme biotransformation. A multi-functional unit composed of the fuel-cell stack and the electro-membrane enzyme reactor could operate independently of external power sources, e.g., in field applications. Possible applications of the integrated fuel-cell stack–EMER units range from biotechnology, chemical synthesis and environmental technology to medical applications.

In this paper selected aspects of an integration of the fuel-cell stack with a prototype EMER are studied experimentally. The voltage–current and the power–current operating curves of the fuel-cell stack and of the enzyme membrane reactor are measured under various operating conditions and mutually compared. The dynamical behaviour of the FCS and the EMER is also assessed.

2. Experimental

2.1. The fuel-cell stack

The experimental fuel-cell stack designated for integration with the EMER consists of nine individual fuel cells with an active cross-sectional area of 26 cm^2 each. To account for the final aim of a portable fuel-cell/EMER system an "open cathode" arrangement is used meaning the stack is supplied with air not from a compressor and a closed piping system but from a simple fan (12 V, max. 2 W) placed at the top of the stack which blows air through open channels at the long sides of the stack. Therefore the air (cathode) side of the stack is always at ambient pressure and

also simultaneously has the function of a heat exchanger (removal of excess heat from inside the stack). Owing to this simple arrangement no feed air humidification is performed.

As the fuel, pure hydrogen is used which is humidified by a simple bubbling in a washing bottle at either ambient or elevated temperature.

In the individual fuel cells a ''monopolar'' plate design (plate material: graphite, thickness 4 mm, supplied by Schunk Kohlenstofftechnik AG, Germany) was used which does not need any gaskets on the active side, but uses the membrane itself as gasket. This plate design is characterized by the fact that each cell is assembled individually outside the stack and held together by nylon screws. Therefore each cell is just a thin graphite plate of 8 mm thickness with outside conventional rubber O-ring gaskets around the hydrogen supply channels. The advantage is that the number of cells in the stack can be varied very easily. This design offers a maximum flexibility, also in terms of intended combination of the fuel-cell stack with the EMER reactor.

The MEAs (membrane electrode assemblies) consist of NAFION^{TM} N-105 membrane (DuPont, USA), onto which catalyst layers are applied. The catalyst used is pure platinum black (unsupported) type HiSPEC1000^{TM} (AlfaAesar-Johnson Matthey GmbH, Germany). The catalyst loading is 1 mg Pt cm^{-2}. In the catalyst layers also a 10 wt.% content (relative to the platinum weight) of NAFION^{TM} polymer is present.

Table 1
Dimensions of the EMER compartments

Compartment	Volume (cm^3)	Thickness (mm)
ec1, ec2	2.8	2.7
rc1, rc2	2.1	2.0
gsc	2.2	2.0

The stack has been manufactured at the Max-Planck-Institute for Dynamics of Complex Technical Systems, Magdeburg.

2.2. The electro-membrane enzyme reactor

The prototype electro-membrane enzyme reactor consists of five flat-shaped compartments manufactured of the acrylic glass or TEFLON plates—see Fig. 1 for the EMER schematism. The basic dimensions of the compartments are either indicated in Fig. 1 or listed in Table 1. The outer dimensions of all plates forming the EMER compartments are adjusted to fit the dimensions of the fuel-cell stack plates (88 mm × 63 mm) in order to enable direct integration of both systems within a single rack.

The outermost compartments (ec1, ec2) are the flow-through electrode compartments where the electrodes delivering the electric field to the reactor are placed. The electrodes are made of the platinized titanium mesh (Magneto-Chemie B.V., The Netherlands). The electrode compartments are continuously rinsed with an electrode buffer.

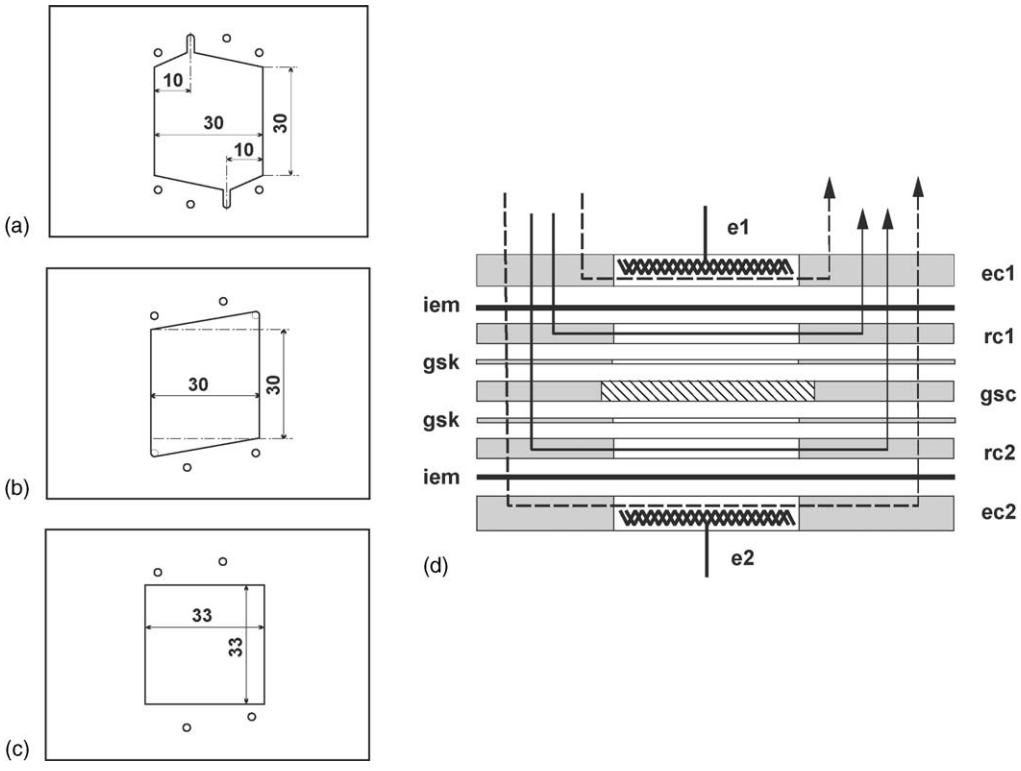

Fig. 1. The schematism of the electro-membrane enzyme reactor. (a) The electrode compartment ec1; (b) the reactant stream compartment rc1, (c) the gel slab compartment. The compartments ec2 and rs2 are mirror images of ec1 and rs1. The dimensions marked in the figures are given in millimeters. The outer dimensions of each compartment are 88 mm × 63 mm and (d) arrangement of compartments in the EMER rack (the rack, the ground plate and the cover plate of the EMER are not depicted for sake of clarity). ec1 and ec2, electrode compartments; rc1 and rc2, reaction stream compartments; gsc, gel slab compartment; e1 and e2, electrodes, gsk, gaskets; iem, ion-exchange membranes; dashed arrows, electrode buffer flows; full arrows, reactant stream flows.

A pair of the flow-through reactant stream compartments (rc1, rc2) delivering the substrate solution to one surface of the gel slab and the washing buffer to the opposite surface of the gel are ''sandwiched'' to the inner surfaces of the electrode compartments. The reactant stream compartments are hydraulically separated from the electrode compartments by a pair of ion-exchange membranes (Ralex AMH-PAD or CMH-PAD, MEGA, Stráž p. Ralskem, Czech Republic) in order to prevent the reactant streams from a contamination by electrode surface reaction products.

The central compartment (gsc) of the EMER holds the gel slab made of the polyacrylamide (5 wt.% of PAA, prepared by the polymerization between two glass plates). The active surface area (exposed to electric field) of the gel membrane is 9 cm^2.

The gaskets made of the rubber-coated fabric SBR AG 2 A (GMS, Lanškroun, Czech Republic) are placed between the reaction stream compartments and the gel slab compartment. All the compartments are equipped with holes forming the channels in the assembled EMER serving for delivery of the liquid streams to the compartments (cf. Fig. 1). The EMER compartments are assembled in a rack between the top and bottom plates (the top plate keeps the inlet and outlet ports) and tightened together by fixing screws. The construction of the EMER enables the thickness and inner arrangement of each compartment to be easily varied to meet the requirements imposed by a specific biotransformation.

2.3. Operating curves of the fuel-cell stack

The voltage–current and power–current operating curves of the fuel-cell stack were measured using the electronic load (STATRON 3229.0, Statron, Germany) for setting the values of the electric current delivered by the fuel-cell stack. The stack voltage after reaching the steady value was measured using the 16-bit data acquisition PC card (PCI-6034E, National Instruments, USA). The hydrogen overpressure at the stack inlet was kept constant (0.3 bar) in all the experiments and the hydrogen was wetted by bubbling through a water in a washing bottle at ambient temperature. The volumetric flow rate of the hydrogen at the stack inlet and the voltage applied to the fan (i.e. the rate of oxygen delivery to the cathodes) were varied in the experiments. The load of the stack, i.e., the value of the electric current density (related to the fuel cells active area) was varied from 0 to approximately 0.3 A cm^{-2}.

2.4. Operating curves of the EMER

The operating curves of the EMER were measured by applying various dc voltages from the stabilized power source (STATRON 2229.81, Statron, Germany) to the reactor electrodes and recording the steady values of the electric current. The current density in the EMER is related to the active area of the gel slab compartment (9 cm^2). The phosphate buffers (pH 8; concentrations: $c_b = 0.01$, 0.025, 0.05 and 0.1 mol dm^{-3}, respectively) were pumped through the reaction stream compartments of the reactor at various volumetric flow rates, Q_b. The electrolytic conductivity of phosphate buffers, κ_b, was measured by laboratory conductivity meter (MultiLab 540, WTW, Germany). The concentrations (and thus also the electrolytic conductivities) of the buffers were chosen in order to mimic reaction conditions in the electro-membrane enzyme reactors used in our previous experiments [13,14]. The electrode compartments of the EMER were washed by the phosphate buffer (pH 8, $c_b = 0.025$ mol dm^{-3}) at a fixed volumetric flow rate of 1 cm^3 min^{-1}. The experiments were performed at ambient temperature.

The polyacrylamide gel membranes placed in the gel slab compartment were soaked with the same buffer as pumped to the reaction stream compartments for at least 12 h prior to mounting the gsc compartment in the reactor. The ion-exchange membranes were also soaked with the same buffer for about 12 h prior to each experiment.

2.5. Dynamics of the EMER

The dynamical behaviour of the electro-membrane enzyme reactor was tested by measuring a response of the electric current passing through the EMER at constant applied voltage after the step change of the concentration of the buffer pumped to the reaction stream compartments. The current values were continuously recorded using the PC data acquisition card (cf. Section 2.3).

3. Results and discussion

3.1. Operating curves of the fuel-cell stack

3.1.1. Effects of the hydrogen volumetric flow rate

The voltage–current operating curves of the fuel-cell stack depicted in Fig. 2 describe the behaviour of the fuel-cell stack

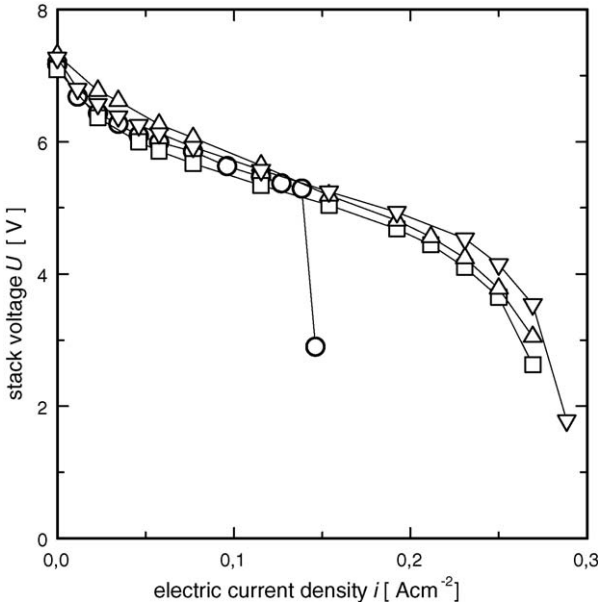

Fig. 2. Voltage–current operating curves of the fuel-cell stack. Humidified hydrogen at overpressure of 0.3 bar was used as the fuel. Hydrogen volumetric flow rate at stack inlet: (○) 10 dm^3 h^{-1}; (□) 30 dm^3 h^{-1}; (△) 40 dm^3 h^{-1}; (▽) 60 dm^3 h^{-1}. The lines in the graph serve only as guides for the eyes.

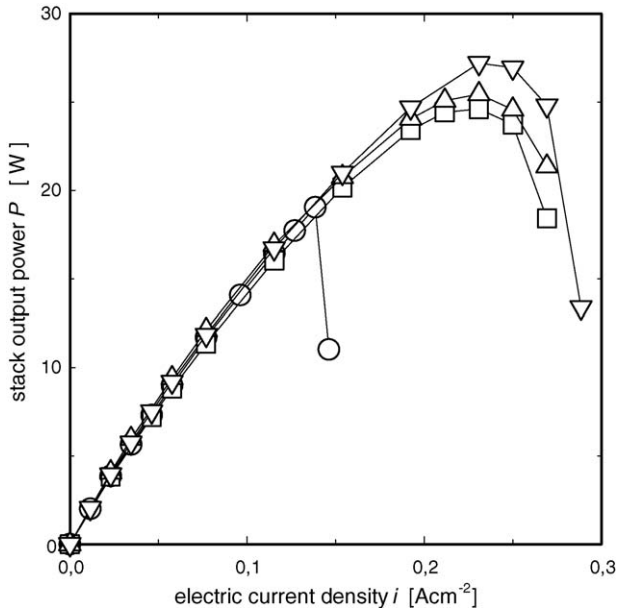

Fig. 3. Power–current operating curves of the fuel-cell stack. Humidified hydrogen at overpressure of 0.3 bar was used as the fuel. Hydrogen volumetric flow rate at stack inlet: (○) 10 $dm^3\ h^{-1}$; (□) 30 $dm^3\ h^{-1}$; (△) 40 $dm^3\ h^{-1}$; (▽) 60 $dm^3\ h^{-1}$. The lines in the graph serve only as guides for the eyes.

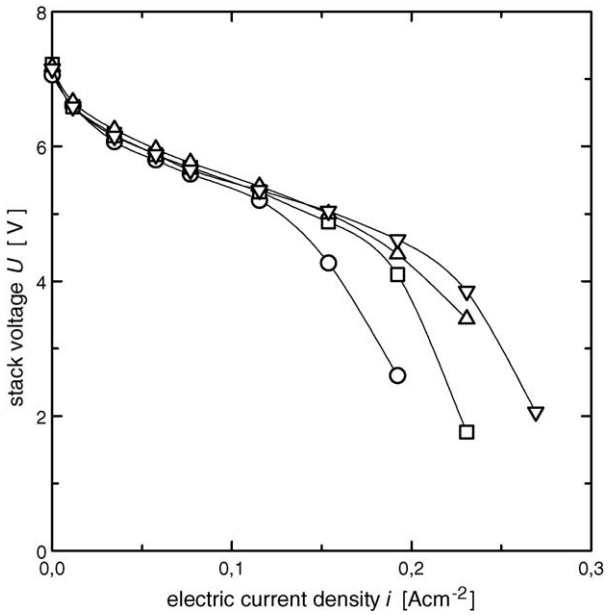

Fig. 4. Voltage–current operating curves of the fuel-cell stack at different air supply rates. Humidified hydrogen at overpressure of 0.3 bar and volumetric flow rate $Q_{H_2} = 40\,dm^3\,h^{-1}$ was used as the fuel. Voltage applied to the air-delivering fan: (○) 7 V; (□) 10 V; (△) 12 V; (▽) 14 V. The lines in the graph serve only as guides for the eyes.

under various hydrogen volumetric flow rates at the stack inlet keeping constant hydrogen overpressure. All current–voltage curves exhibit very similar shapes over the entire range of the current densities at all hydrogen flow rates, except the lowest flow rate, $Q_{H_2} = 10\,dm^3\,h^{-1}$, when the curve exhibits a steep decrease of the stack output voltage at the current density of about 0.13 A cm^{-2}. The stack output power falls accordingly—cf. Fig. 3. A depletion of the hydrogen at the anode side of the fuel cells is the reason for the observed behaviour of the fuel-cell stack at the lowest hydrogen volumetric flow rate. The volumetric flow rates of the hydrogen higher than approximately 30 $dm^3\ h^{-1}$ have obviously only marginal effects on the voltage–current and power–current operating curves. It can be concluded that the fuel-cell stack can be operated at the lowest hydrogen volumetric flow rate used in the experiments (10 $dm^3\ h^{-1}$) if the current load is kept below approximately 0.13 A cm^{-2}. When higher current loads are to be used the hydrogen volumetric flow rate has to be increased accordingly, say to 25–30 $dm^3\ h^{-1}$. Under the given mode of the FCS operation (defined mainly by the way of hydrogen humidification and its overpressure at the stack inlet) the maximum output power achieved was about 25 W at the electric current density of about 0.25 A cm^{-2} and at the stack voltage of about 4 V.

3.1.2. *Effects of the air supply rate*

The rate of air supply to the cathodes of the fuel cells is defined by the rotational speed of the fan mounted at the top of the fuel-cell stack. The speed of the fan rotation is determined by the voltage applied to the fan, U_f. Figs. 4 and 5 document strong effects of the air supply rate on the operating curves at the electric current densities above approximately 0.125 A cm^{-2}. At lower current loads the speed of the fan rotation has practically no effect on the operating curves. The maximum output power of the fuel-cell stack varies between 17 and 24 W when the fan voltage is changed from 7 to 14 V (see Fig. 5).

The experimental results shown in Figs. 2–5 (and also other results not shown in this paper) proved that the operating curves of the fuel-cell stack are only slightly affected by the operating

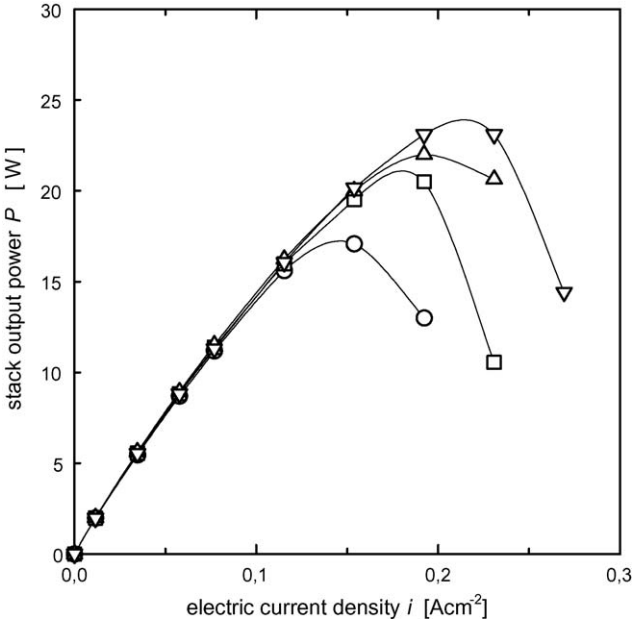

Fig. 5. Power–current operating curves of the fuel-cell stack at different air supply rates. Humidified hydrogen at overpressure of 0.3 bar and volumetric flow rate $Q_{H_2} = 40\,dm^3\,h^{-1}$ was used as the fuel. Voltage applied to the air-delivering fan: (○) 7 V; (□) 10 V; (△) 12 V; (▽) 14 V. The lines in the graphs serve only as guides for the eyes.

conditions (the hydrogen flow rate, the air flow rate, the way of hydrogen wetting, the hydrogen overpressure) if the stack load is below 50% of its maximum load, i.e., below electric current density of approximately 0.15 A cm^{-2}.

3.2. Operating curves of the EMER

The experimental voltage–current and power–current operating curves of the electro-membrane reactor measured at four concentrations of the buffer (covering the range of the electrolytic conductivities of reaction streams in our previous experiments [13,14]) pumped to the reaction stream compartments at the constant volumetric flow rate, Q_{rc} = 1.0 cm^3 min^{-1}, are shown in Fig. 6. The volumetric flow rate of 1.0 cm^3 min^{-1} corresponds to the Reynolds number value, $Re_{rc} = d_h v\rho/h$ = 2.2, i.e., the buffer flow is strictly laminar and mass transfer resistances at the solid–liquid interfaces would dominate the overall mass transport resistance. The operating curves clearly document a non-ohmic character of the EMER electrical resistance. The increase of the electric current density with the increasing voltage applied to the reactor is negligible at applied voltages up to approximately 2 V (Fig. 6). Then, the electric current increases with the increasing voltage in an almost linear manner. The value of the current passing through the EMER is strongly influenced by the buffer electrolytic

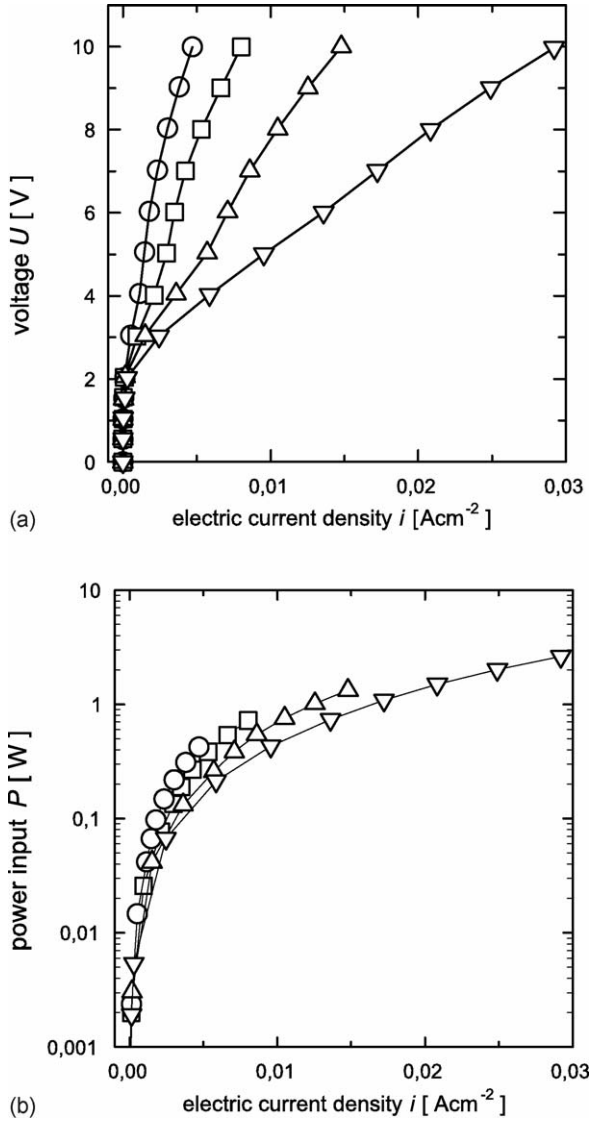

Fig. 6. Operating curves of the EMER at different buffer concentrations. (a) Voltage–current operating curves, (b) power–current operating curves. Buffer concentration and specific electrolytic conductivity: (○) 0.01 mol dm^{-3}, 1.7 mS cm^{-1}; (□) 0.025 mol dm^{-3}, 4.0 mS cm^{-1}; (△) 0.05 mol dm^{-3}, 7.3 mS cm^{-1}; (▽) 0.1 mol dm^{-3}, 12.7 mS cm^{-1}. Volumetric flow rates in reaction stream compartments: Q_{rc} = 1.0 cm^3 min^{-1} (Re_{rc} = 2.2), volumetric flow rates in electrode compartments: Q_{ec} = 1 cm^3 min^{-1}. The lines in the graphs serve only as guides for the eyes.

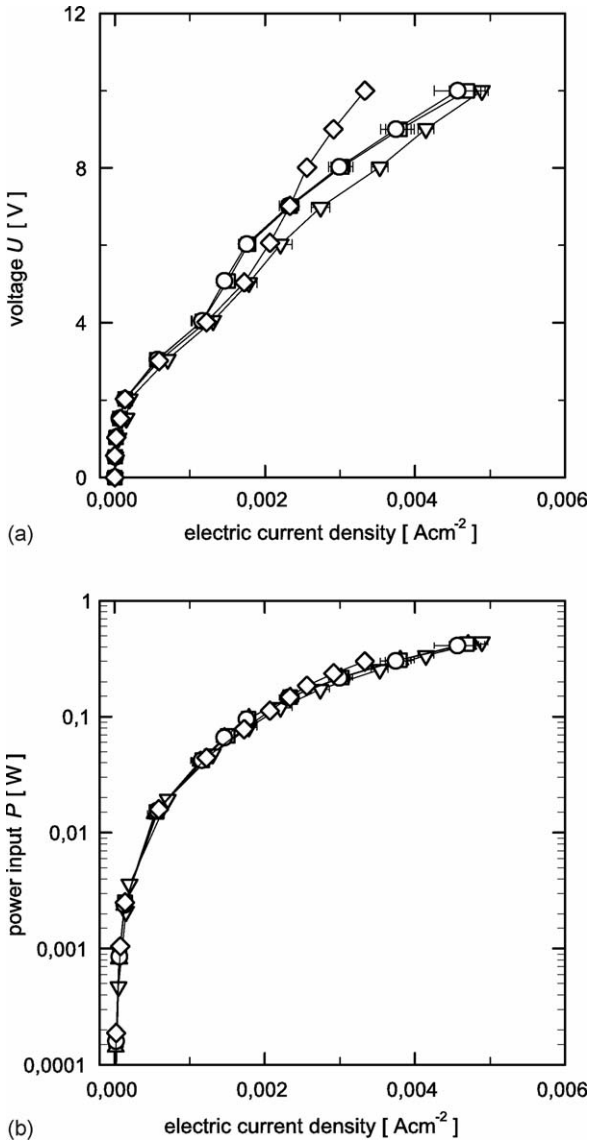

Fig. 7. Operating curves of the EMER at various buffer flow rates. (a) Voltage–current operating curves, (b) power–current operating curves. Volumetric flow rates in reaction stream compartments: (○) 0.5 $cm^3 min^{-1}$ (Re_{rc} = 1.1); (□) 0.75 cm^3 min^{-1} (Re_{rc} = 1.7); (△) 1.0 cm^3 min^{-1} (Re_{rc} = 2.2); (▽) 5 cm^3 min^{-1} (Re_{rc} = 11.1); (◇) 10 cm^3 min^{-1} (Re_{rc} = 22.3). Buffer concentration and specific electrolytic conductivity: c_b = 0.01 mol dm^{-3}, κ_b = 1.7 mS cm^{-1}. Volumetric flow rates in electrode compartments: Q_{ec} = 1 cm^3 min^{-1}. The lines in the graphs serve only as guides for the eyes. The errorbars show the interval of ±one standard deviation.

conductivity. In a system combining the EMER and FCS the resistance of the reactor part thus can be adjusted by changing the concentration of a buffer used for the substrate stream preparation. The power input–current density operating curves of the EMER are shown in Fig. 6b. The power consumption of the reactor was always lower than 2 W, i.e., below about 10% of the fuel-cell stack maximum power output. The current density values delivered to the EMER by the fuel-cell stack at its maximum voltage (approximately 7 V) range from 2.5 to 18 mA cm^{-2}. This range of current densities has been found sufficient for effective control of the penicillin G hydrolysis in our experimental EMERs [13,14].

The operating curves of the electro-membrane reactor at various flow rates of the buffer pumped to the reactant stream compartments are shown in Fig. 7 ($c_b = 0.01$ mol dm^{-3}, $\kappa_b = 1.7$ mS cm^{-1}) and Fig. 8 ($c_b = 0.1$ mol dm^{-3}, $\kappa_b = 12.7$ mS cm^{-1}). The operating curves cover the same voltage and current density ranges as the curves depicted in Fig. 6. The electrical behaviour of the EMER is only slightly influenced by the buffer velocity in the reactant stream compartments (especially at higher buffer electrolytic conductivity) as the flow regime within the compartments is laminar at all flow rates: $Re_{rc} \in \langle 1.1, 22.3 \rangle$. This observation is of great importance as the EMERs can be operated at vastly different flow rates in the reactant stream compartments depending on the mode of the reactor operation (circulation versus flow-through mode [13,14]), rate of the biotransformation performed, etc.

Mutual comparison of operating curves of the fuel-cell stack and the EMER in Figs. 2–8 indicates that the operating curves of the EMER prototype examined in this paper span only the leftmost region of the operating curves of the fuel-cell stack, i.e., the electric power consumed by the EMER represents only up to about 10% of the power output of the fuel-cell stack.

In practical applications of a multi-functional unit combining the EMER and the fuel-cell stack, a knowledge of the dynamical behaviour of both sub-units is also of great importance with respect to the determination of the rate controlling step. The experimental data presented in Fig. 9a and b show responses of both sub-units to the step changes of their key operational parameters: the buffer concentration (electrolytic conductivity) in the case of the EMER and the current load in the case of the FCS. The curves in Fig. 9a suggest that the characteristic response times (time constants) of the EMER (without a biotransformation) are in the order of several hours owing to low (diffusional and electrophoretic) transport rates in all the compartments. The dynamics of the fuel-cell stack is substantially faster, its characteristic times are in the order of a few minutes [9]. We can speculate that in the coupled system the rate of a biotransformation will be predominantly controlled by the mass transport rates [13,14] or, possibly in the case of very slow biotransformation, by the reaction kinetics. The dynamics of the FCS would not become a rate controlling factor in the coupled multi-functional unit.

In this paper we have studied experimentally only electrical operating curves of both sub-units intended for an integration. A question may arise on the practical applicability of the coupled FCS–EMER system for practical enzyme biotransformations. Therefore we recall here briefly results of our previous studies [13,14] obtained with two laboratory electro-membrane reactors (of the same kind as the reactor depicted in Fig. 1) differing markedly in dimensions of their enzymatically active compartments (cf. caption to Fig. 10). A hydrolysis of penicillin G by penicillin G acylase (immobilised in polyacrylamide membranes) has been used as a testing biotransformation. Penicillin G (PenG) is split to phenylacetic acid (PAA) and 6-aminopenicillanic acid (6-APA) in this reaction. Hydrogen ions are also produced owing to the immediate PAA dissociation. PenG, PAA and 6-APA are all present as anions in the reaction environment. All reaction components

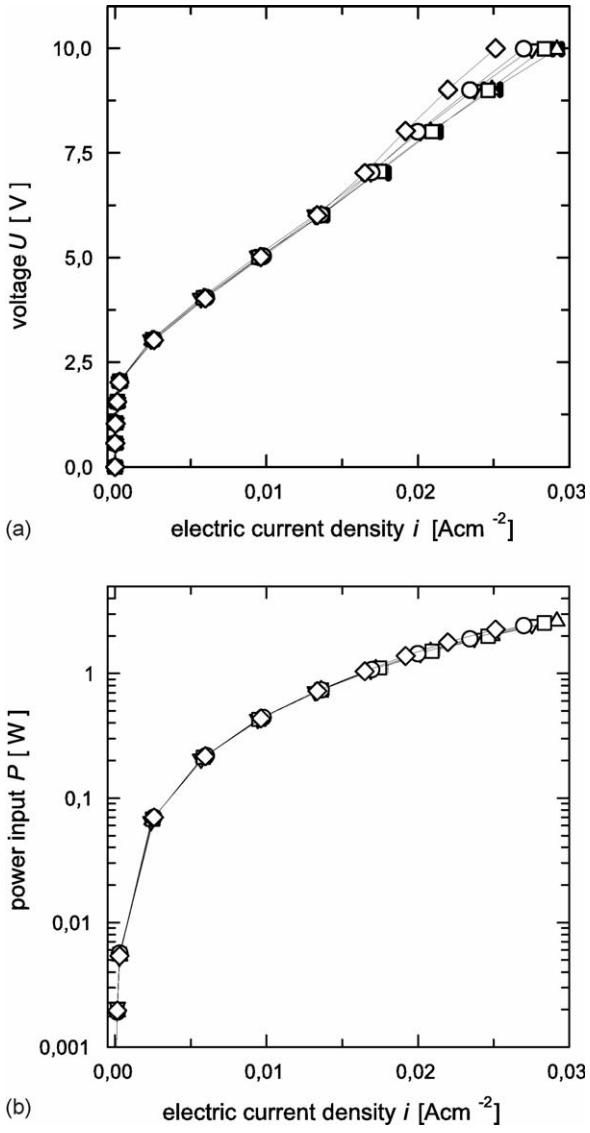

Fig. 8. Operating curves of the EMER at various buffer flow rates. (a) Voltage–current operating curves, (b) power–current operating curves. Volumetric flow rates in reaction stream compartments: (○) 0.5 cm^3 min^{-1} ($Re_{rc} = 1.1$); (□) 0.75 cm^3 min^{-1} ($Re_{rc} = 1.7$); (△) 1.0 cm^3 min^{-1} ($Re_{rc} = 2.2$); (▽) 5 cm^3 min^{-1} ($Re_{rc} = 11.1$); (◇) 10 cm^3 min^{-1} ($Re_{rc} = 22.3$). Buffer concentration and specific electrolytic conductivity: $c_b = 0.1$ mol dm^{-3}, $\kappa_b = 12.7$ mS cm^{-1}. Volumetric flow rates in electrode compartments: $Q_{ec} = 1$ cm^3 min^{-1}. The lines in the graphs serve only as guides for the eyes. The errorbars show the interval of ±one standard deviation.

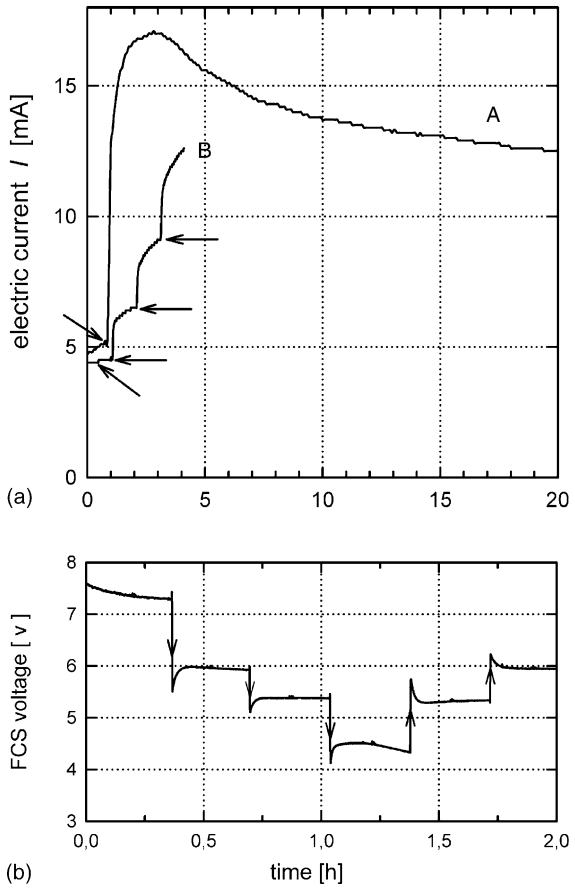

Fig. 9. Dynamics of the EMER (a) and of the fuel-cell stack (b). The curve A in panel (a) shows the current density response of the EMER after the step change of the buffer concentration from 0.01 to 0.1 mol dm^{-3}; the curve B shows the current density responses of the EMER after subsequent step changes of the buffer concentration: 0.01 → 0.025 → 0.05 → 0.1 mol dm^{-3}. The applied voltage was kept constant (3 V) in all cases. The arrows point to instants of buffer concentration switching. The line in panel (b) shows the fuel-cell stack voltage responses to changes in the stack current load. The load was changed by 1A steps at time instants indicated by the arrows.

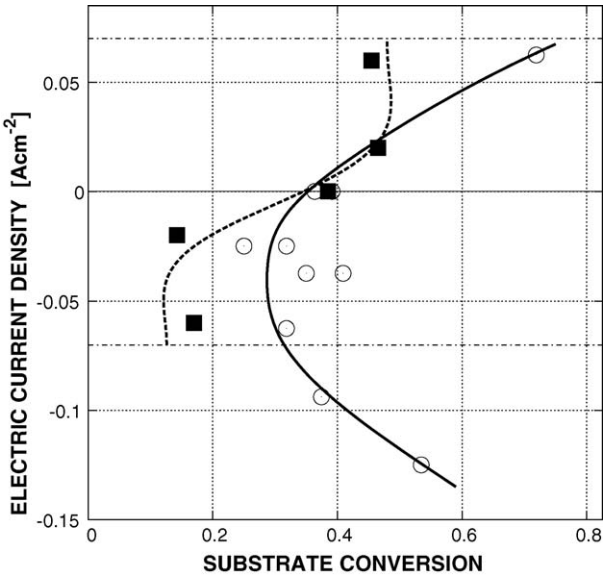

Fig. 10. Electric current density as a function of required substrate conversion in experimental electro-membrane enzyme reactors. (☉) (solid line), batch reactor [13] (membrane material: 5% polyacrylamide gel; membrane active area: 40 mm × 40 mm; membrane thickness: 2.7 mm; membrane enzyme activity: 30 U cm^{-3}; substrate concentration: 2% (w/v); reaction temperature: 37 °C); reaction time: 6 h. (■) (dashed line), continuous flow-through reactor [14] (membrane material: 5% polyacrylamide gel; membrane active area: diameter 10 mm; membrane thickness: 2.6 mm; membrane enzyme activity: 24 U cm^{-3}; substrate concentration: 2% (w/v); mean residence time: 1 h; reaction temperature: 30 °C). Enzyme reaction: penicillin G splitting by penicillin G acylase. Dash-and-dot lines delimit interval of electric current densities attainable in the prototype multi-functional unit studied in this paper.

can therefore be transported by electrophoretic migration when an electric field is applied to the reactor. First the electro-membrane reactor used in the experiments was operated in a batch (circulation) mode, the second one was operated in a continuous flow-through mode—experimental details are given in the caption to Fig. 10. The curves in Fig. 10 clearly indicates that the value of the substrate conversion (i.e., also of the reaction rate) can be controlled across a wide interval by the magnitude of the electric current applied to the reactors. The shapes of the curves can be explained by mutual interactions of non-linear kinetics of the enzyme reaction, pH dependence of reaction rate and electrophoretic and diffusional transport of reaction components within the gel membrane with the immobilised enzyme (see [13,14] for details). The dash-and-dot lines in Fig. 10 indicates the maximum electric current density value attainable in the prototype coupled FCS–EMER system reported in this paper. The interval of attainable electric current density values is somewhat narrower compared to the interval used in our previous experiments [13,14]. Nevertheless, the plots in Fig. 10 prove the applicability of the coupled system for practical enzyme biotransformations (keeping also in mind differences in dimensions of compartments of the EMER studied in this paper and of the EMERs reported in Fig. 10).

4. Conclusions

The experiments, although performed with separated (not physically integrated) parts of the proposed coupled unit, have demonstrated both the viability and the feasibility of the idea of assembling a multi-functional unit utilizing the electric current as the coupling tool between the sub-units. The coupling of the sub-units can be done via external wiring, however, we aim to the direct ''sandwiching'' of the sub-units within a common rack in the future. Such an arrangement will allow not only for the electric coupling but heat integration will be also possible.

The power output of the fuel-cell stack has vastly surpassed the power demand of the EMER. There is, even when considering certain modifications of the EMER design (e.g., an increase in its active cross-sectional area or a parallelization of the compartments) a considerable surplus electric energy production that could be used, for example, to drive the pumps delivering substrate and buffer streams to the reactor.

In conclusion, we can state that the question in the title of this paper can be answered: yes, the fuel-cell stack and the electro-membrane enzyme reactor can be combined within a multi-functional unit. The present study has proved the electrical

compatibility of both sub-units and the results of our previous experimental studies have also evidenced their compatibility from the point of view of enzyme biotransformations.

Acknowledgments

The authors thank the Ministry of Education of the Czech Republic (Grants: ME666-KONTAKT Programme and MSM 6046137306) and the Bundesministerium für Bildung und Forschung (WTZ-Projekt: CZE 02/024) for financial support. RK thanks the Czech Science Foundation for additional support (Grant No.: 104/03/H141).

References

[1] D.W. Agar, W. Ruppel, Chem.-Ing.-Tech. 60 (1988) 731.
[2] K.R. Westerterp, Chem. Eng. Sci. 47 (1992) 2195.
[3] E.J. Houdry, GB Patent 579,477, 1944.
[4] E.J. Houdry, US Patent 2,419,997, 1947.
[5] E.H. Stitt, Chem. Eng. Res. Des. 82 (A2) (2004) 129.
[6] U. Hoffman, K. Sundmacher, Chem.-Ing.-Tech. 69 (1997) 613.
[7] D.W. Agar, Chem. Eng. Sci. 54 (1999) 1299.
[8] F.M. Dautzenberg, M. Mukherjee, Chem. Eng. Sci. 56 (2001) 251.
[9] J.G. Sanchez-Marcano, T.T. Tsotsis, Catalytic Membranes and Membrane Reactors, Wiley–VCH, Weinheim, 2002.
[10] M. Přibyl, P. Hasal, M. Marek, Chem. Biochem. Eng. Q. 12 (1998) 141.
[11] M. Přibyl, R. Chmelíková, P. Hasal, M. Marek, Chem. Eng. Sci. 56 (2001) 433.
[12] M. Přibyl, R. Chmeliková, P. Hasal, M. Marek, J. Chem. Technol. Biotechnol. 77 (2002) 51.
[13] M. Přibyl, R. Chmelíková, M. Marek, Enzyme Microb. Technol. 33 (2003) 793.
[14] A. Zadražil, R. Chmelíková, P. Hasal, Biotechnol. Lett. 25 (2003) 485.
[15] K. Kordesh, G. Simader, Fuel Cells and Their Applications, VCH, Weinheim, 1996.
[16] J. Larminie, A. Dicks, Fuel Cell Systems Explained, Wiley–VCH, Weinheim, 2003.